THE JOURNAL OF PHYSICAL CHEMISTRY A

 VOLUME 106, NUMBER 43, OCTOBER 31, 2002

FEATURE ARTICLE

Photodissociation of Hydrogen Halide Molecules in Different Cluster Environments

Udo Buck*

Max-Planck-Institut für Strömungsforschung, Bunsenstrasse 10, D-37073 Göttingen, Germany

Received: March 25, 2002; In Final Form: July 30, 2002

The photodissociation of molecules and the interaction of the products with the surrounding cage atoms is an important field of research in solvation dynamics. The targeted generation of clusters with known size distributions and the placement of molecules on the surface or in the interior of these clusters allows us to carry out such investigations for finite systems as function of the size. We will present results of the photodissociation of HBr and HI molecules at 243 nm interacting with different rare gas clusters Ne_n, Ar_n, Kr_n, and Xe_n in the size range from $n = 50$ to 830. We mainly measure the kinetic energy of the outgoing H atoms in a time-of-flight mass spectrometer. The amount of fast, unperturbed or slow, caged and recombined H atoms depends strongly on the site, the special surface state, the cage material, the cluster size, and the kinetic energy available. The results are compared with calculations using mixed quantum-classical methods. In the photodissociation of HI in Xe_n clusters we observed the formation of HXeI that belongs to a recently discovered class of ionically bound systems. It is detected by the orientation in combined strong laser and weak electric fields. In small complexes $(HBr)_x$ that were deposited in and on large rare gas clusters either vibrations or rotations were exited depending on their site and size.

Introduction

The photodissociation of molecules in condensed media is the object of extensive experimental and theoretical efforts in chemical reaction dynamics. In particular, the influence of the solvent on the unimolecular fragmentation mechanisms plays a crucial role in the cage effect, where the interaction with the solvent leads eventually to recombination and relaxation to the ground state.[1] Experiments have been carried out in solids,[2] liquids,[3] and high-pressure gases[4] using a large variety of methods ranging from classical kinetics over laser spectroscopy to real time dynamics in the femtosecond regime.[5] Despite these efforts information on the specific underlying molecular models is difficult to get, since the experimental information is often restricted by averaging processes and the theoretical interpretation is hampered by the problem of solving the many-body quantum system.

* To whom correspondence should be addressed. E-mail: ubuck@gwdg.de.

At this point clusters come into consideration. There are several advantages and specific attractions in using clusters as media for exploring the influence of the cage. (1) The number of constituents is finite as is the number of degrees of freedom. This leads usually to a well defined system that should greatly facilitate the calculation.[6] (2) The properties can be investigated as a function of the size. This fact allows us, for example, to study the influence of the different solvent shells on the molecule. In the two limiting cases we expect for the 1:1 complexes the molecular and for several hundred atoms the bulk behavior. (3) In clusters we have access to special experimental observables that are otherwise difficult to obtain. An example is the measurement of the kinetic energy of the molecular fragments that is not available in experiments in matrixes or liquids.

In Figure 1 we show pictorially what can happen to a HI molecule that is embedded in the cluster, freely rotates, and is

10.1021/jp0208079 CCC: $22.00
Published on Web 09/28/2002

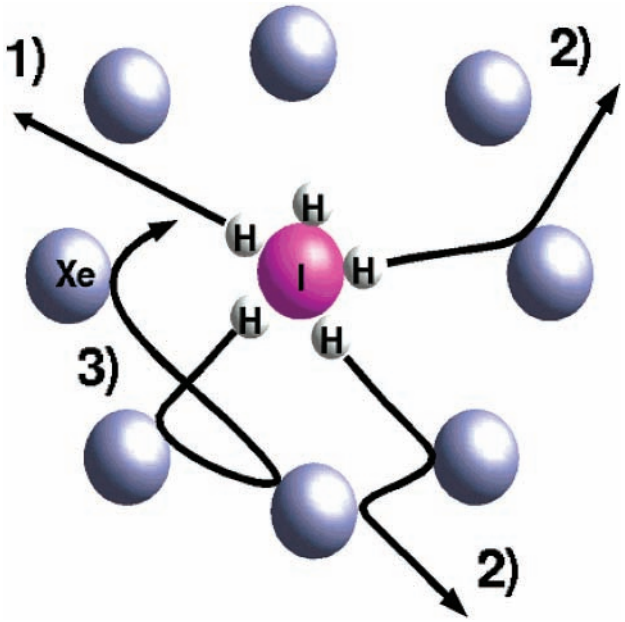

Figure 1. Schematic view of the possible reaction paths of photodissociated HI molecules. (1) direct cage exit, (2) delayed cage exit after several collisions, and (3) complete caging.

photodissociated. (1) In the *direct cage exit* the H atom leaves the cluster without being disturbed by the surrounding cage atoms with the velocity corresponding to the dissociation of the free molecule. (2) The most probable case seems to be the *delayed cage exit* where the H atom interacts one or two times with the cage atoms and leaves the cage with lower velocity than in case (1). (3) Finally, there is the possibility to interact so often with the cage atoms that the outgoing H atom loses its energy completely and is ready for recombination, the *cage effect*. We also note that for clusters new phenomena appear that are not found in bulk liquids or solids and that are connected with the fact that clusters have large surface areas and low temperatures. The former feature leads to a strong dependence of the cage effect on the position on the surface and the latter one magnifies the importance of quantum effects in the vibration−rotational motion of the molecule.[7]

The systems among the solvated diatomic molecules that have attracted most interest by the theoreticians are the hydrogen halide molecules HX interacting with rare gas clusters Rg_n. They have been extensively studied using various theoretical approaches.[7−19] The reason for this preference is obvious. For these systems very accurate potential energy surfaces of the ground state are available. They are obtained from high-resolution spectroscopy of the van der Waals complexes and high quality surfaces are known, for instance, for HF−, HCl−, HBr−, HI−Ar, and HCl−Ne.[20−26] In addition, the hydrogen halides exhibit a rich and interesting behavior in the electronically excited states where 12 states are coupled leading asymptotically to the population of the ground X and excited spin−orbit state X* of the halide atoms. The increasing influence of the spin−orbit coupling when going from HF to HI results in a different behavior of the angular distributions and the branching ratios of the final states after the photodissociation process. Some of the details will be discussed in section III.A.

The results of the calculations with clusters demonstrate that in small clusters the products are barely hindered in the dissociation process. The picture changes with the first fully solvated shell which occurs around $n = 13$. Here, the H atoms exhibit clear indications of the cage effect and appear in the kinetic energy distribution with nearly zero velocity. With the closure of the second icosahedral shell at $n = 55$ these effects become more pronounced. But we note that also in this size range, depending somewhat on the system and the type of calculation, there still exist fast H atoms which manage to leave the cage directly so that a bimodal distribution results. A new perspective was introduced by Niv et al.[14] who showed that for $HCl-Ar_{12}$ the cage effect is more pronounced when the HCl molecule is sitting on the surface of the Ar cluster instead of being placed inside. This configuration turned out to be the global minimum of the potential surface[12,27] which is separated by a high barrier from the embedded isomer. Similar conclusions, although quantitatively different, were drawn in a recent investigation of $HBr-Ar_{12}$ clusters.[7] We conclude that the simple rule that fast products originate from surface and slow ones from interior positions does not hold for these systems.

Given these detailed results from theory, we should ask the question of what can be realized experimentally. The most detailed results are still obtained with molecular ions embedded in inert argon or carbondioxide clusters.[28,29] For neutral systems, nitrite,[30−32] methyliodide,[33,34] and OClO[35,36] clusters were investigated. In two recent studies on OClO[37] and HNO_3[38] molecules in different cluster environments, the velocity or the internal state distribution of the photofragments were measured. For neutral hydrogen halide clusters either small complexes[39−41] or large neat clusters with unknown size distribution[42] were measured. We tried to solve the problem for $(HBr)_n$ clusters[43,44] by determining the average cluster size distribution by applying the atomic beam deflection method.[45] We observed indeed the indication of a cage effect for average cluster sizes $\langle n \rangle \geq 6$ at a dissociation wavelength of 243 nm.[46] It disappeared when we used 193 nm for the dissociation wavelength. In this case the available kinetic energy is larger. The experimental tool was, among other observables, mainly the kinetic energy distribution of the outgoing H atoms.

On the bases of these results, we started a series of measurements on the hydrogen halide−rare gas systems. This article is an account of these recent studies by my group of the photodissociation of HBr and HI molecules embedded in or adsorbed on large rare gas clusters in the size range from $\langle n \rangle =$ 50 to 830. In this way we will be able to answer questions as follow. What is the amount of direct cage exit, delayed cage exit, and completely caged events? How do they depend on the internal and the different surface states? What is the role of the rare gas host concerning the mass and the size? What has to be accounted for in the calculations to get agreement between experiment and theory?

The paper is organized as follows. I will start with an overview of the experimental and theoretical methods applied. Then I will present the results of single HBr and HI molecules in different cluster environment. The report on the detection of the molecule HXeI that belongs to a newly discovered class of ionically bound molecules follows.[47] It is formed in the photodissociation of HI molecules on the surface of large Xe_n clusters. Finally I will also show results for small complexes $(HBr)_x$ from $x = 2$ to 8 deposited inside or on the surface of large rare gas clusters[48] and compare the results with those obtained for pure $(HBr)_x$ clusters with $\langle x \rangle = 8$.[46] Here interesting collision effects occur, since the neighbor molecules are vibrationally and rotationally excited by the fast H atoms in their constraint geometries. The paper is finished by a summary and a discussion of future prospects of the methods.

II. Experimental Methods

The basic experimental technique for almost any photodissociation experiment with clusters is a molecular beam apparatus

with an adiabatic expansion to generate the clusters, a buffer chamber for manipulating them, and a time-of-flight mass spectrometer for the detection that also contains the ports for the dissociation laser. We will discuss the important elements for our experiments separately.

A. Preparation of Surface and Embedded Molecules and Complexes. The rare gas host clusters are produced by isentropic expansions through nozzles of conical shape. By varying pressure and temperature of the source the average size is easily shifted from $\langle n \rangle = 50$ to 830. The clusters in this size range usually form a log-normal distribution that is nowadays directly measured by fragmentation free[49] or fragmentation corrected[50] methods. The resulting average sizes are correlated with the source parameters based on the ideas of Hagena.[51] The resulting parameters for rare gas clusters are well-known, since they were mainly used as prototype systems for testing the scaling laws. They can be found in refs 50, 52, and 53. In this way the rare gas cluster sizes are known from their production conditions.

To prepare embedded or adsorbed molecules with these clusters two different techniques are applied. In the former case, a coexpansion of the molecule and the host gas is used. Since hydrogen halide molecules form, because of the higher binding energy, much more easily clusters with themselves than with the rare gas atoms, one has to go to very dilute mixtures to reach the limit of one molecule in a rare gas cluster. In case of HBr, a 5% mixture in argon produces pure $(HBr)_n$ clusters with the average sizes around $\langle x \rangle = 8$, since the released binding energy of the molecular clusters is used to evaporate all argon atoms.[43] Therefore we had to go to very dilute mixtures of at least 0.1% HBr in Ar and low source temperatures, in this case 229 K, to place a single HBr molecule inside the Ar_n cluster with $\langle n \rangle = 100$.[17] Both results were carefully checked, in this case by a combination of scattering and mass spectrometer analysis. It is obvious from what has been said that there is the possibility to operate the source between these two cases. For a larger amount of HBr molecules and a smaller amount of Ar atoms, the released binding energy is not high enough to evaporate all Ar atoms and mixed clusters of the type $(HBr)_xAr_n$ result with x in the range 1−8.

The preparation of adsorbed molecules is realized by the so-called pick-up technique introduced by Scoles and co-workers.[54] The cluster is passed through a small scattering cell filled with the molecular vapor with variable pressure in the range of 10^{-2} mbar as is shown in Figure 2. The number of molecules captured depends sensitively on this pressure and follows a Poisson distribution.[55] A typical example, again for HBr, is also depicted in Figure 2. Here the measured number of monomers and dimers is plotted against the cell pressure. They follow nicely the calculated Poisson curves. By a suitable choice of the source pressure, one can easily arrange conditions at which only one molecule is adsorbed on the surface of the cluster. Usually the probability to penetrate inside the cluster is small, since very often the surface state is a local minimum on the potential surface separated by a large barrier from the embedded state. Recently Vach carried out extensive molecular dynamics simulations on this process.[56] He observed as a rule of thumb that the probability of the molecule for going inside decreases with increasing minimum distance and decreasing well depth of the local interaction. Typical examples are Xe and SiF_4 that stay preferentially close to the surface of the argon cluster in the size range of $n = 100$ and SF_6 that goes inside into a matrix state. One can estimate from these results and a series of new calculations[57,58] that HBr on Ar_n stays near the surface in the first and second shell, while HI starts to penetrate inside and resides mainly in the second shell. In the same way, we are also able to produce small complexes on the cluster surface whose amount is known by the Poisson distribution.[48]

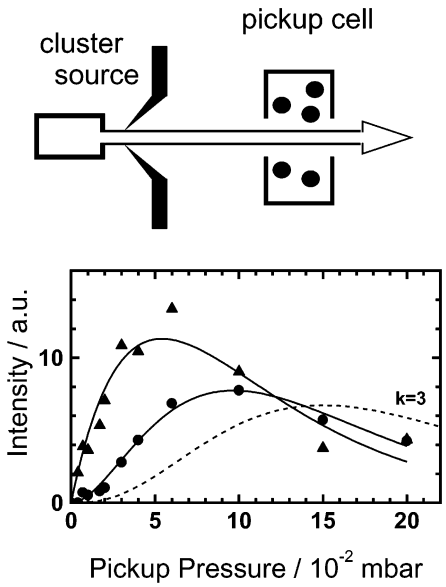

Figure 2. Schematic view of the pick-up arrangement and typical results for HBr monomers (triangles) and dimers (circles). The lines are calculated Poisson distributions.

B. Detection of H Atoms and Velocity Analysis. The field of photodissociation of bare molecules is very well developed with a number of sophisticated detection techniques ranging from Doppler and time-of-flight spectroscopy[59,60] over laser induced fluorescence[60] to the photofragment imaging techniques.[34,61] We are in particular interested in the detection of H atoms. For these atoms Welge and co-workers[62] have demonstrated the elegant technique of Rydberg tagging. Instead of ionizing the nascent neutral H atom by a resonance enhanced multiphoton (REMPI) process, the H atoms are excited to a high Rydberg state and fly as neutrals to the detector where they are ionized by a small electric field. In this way high sensitivity is combined with high resolution. Since we are interested in detecting H atoms with small and even zero velocity, we have to apply more conventional techniques where the translational distribution of the neutral photofragments are monitored by the ion. By applying a small electric field we extract those ions already flying in the direction of the detector and turn around those ones that start in the opposite direction. From the different arrival times the velocity is calculated.[63]

Our experimental arrangement for the detection is schematically shown in Figure 3. The molecules in or on the cluster beam are dissociated by a focused pulsed laser beam of 243.06 nm and 10 ns duration. By changing the polarization of the laser, the angular dependence of the photodissociation is measured. The ionization takes place with the same laser pulse in a (2+1)-REMPI scheme. The ions are extracted by a small electric field of 4 V into a two-stage time-of-flight mass spectrometer (TOFMS) of the Wiley−McLaren type.[64] It is surrounded by a copper shield mounted on a high-pressure helium compressor at 20 K to suppress the H atom background from hydrocarbons. At the interaction point, the molecular beam, the dissociation laser beam, and the TOFMS collection axis are oriented mutually perpendicular to each other. Thus Doppler effects are eliminated in the photodissociation measurements.

What is actually measured in the experiment is the kinetic energy of product H atoms by analyzing the trajectories of the

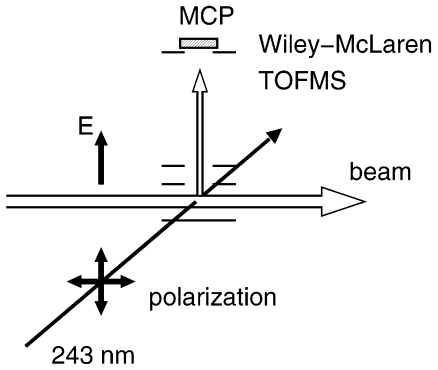

Figure 3. Schematic view of the detector arrangement.

ions. As already mentioned, operating the TOFMS in the so-called low-field mode causes a splitting of the peaks originating from ions which are directly ejected toward the detector and those which first move in the opposite direction, are decelerated in the extraction field and then return. In this way we are able to detect slow fragments, even with zero kinetic energy, which give rise to a signal exactly centered between the peaks of the fast ions.

The different contributions which can be derived from the measured kinetic energy of the H atom $E_{kin}(H)$ are best discussed by the energy balance of the process

$$h\nu + E_{int}(HBr) = D_0 + E_{int}(Br) + E_{kin}(Br) + E_{kin}(H) + E_{clu} \quad (1)$$

where the excitation wavelength $h\nu$ and the dissociation energy D_0 of HBr are known, and $E_{kin}(H)$ is measured. By conservation of momentum, the kinetic energy of the Br atoms $E_{kin}(Br)$ is also known. The excitation of the spin−orbit state Br* in the Br product channel is presented by $E_{int}(Br)$ and is measured as energy loss in the kinetic energy of the H atom $E_{kin}(H)$. These effects would also appear in the dissociation of HBr monomers and indicate the direct cage exit (1). The influence of the cluster is expressed by the continuous energy loss E_{clu} of the H atoms caused by the collisions with the cage. This leads, depending on the position, to delayed cage exit or complete caging (2). The internal excitation of the HBr molecule before the dissociation $E_{int}(HBr)$ is observed as energy gain (3). In general, the molecules will be in the ground state after the expansion. There are, however, two possibilities to observe internally excited molecules. One is the existence of recombined molecules that are quite hot. The other might occur in small complexes where a fast already dissociated H atom collides with its neighbor molecule and excites it according to H + HBr → H + HBr*.

A typical measurement of a time-of-flight distribution that exhibits all these features is shown in Figure 4. It is obtained after the dissociation of $(HBr)_8$.[46] The structure is, as expected, nearly symmetric (not completely because the two groups of ions pass through slightly different field configurations). We recognize three structures as follows: (1) The two large peaks correspond with their very small satellites to the direct cage exit into the H+Br and H+Br* channels, respectively. (2) The small peak in the middle corresponds to H atoms with zero velocity. (3) The features beyond the cage exit peaks are due to vibrationally excited HBr molecules.

We note that the process of slowing the H atoms transfers an appreciable amount of energy to the cage so that the cluster starts to evaporate.[10] This makes the detection of H atoms with

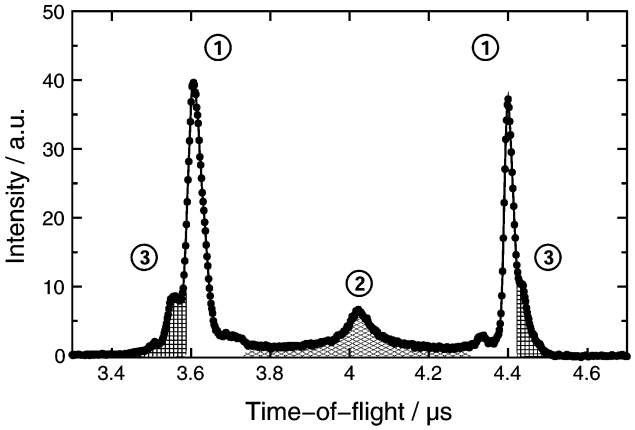

Figure 4. TOF spectrum of H atoms from the dissociation of $(HBr)_n$ clusters with $\langle n \rangle = 8$. (1) direct cage exit, (2) slowed and caged atoms, and (3) vibrationally excited molecules.

small velocities much easier so that most of them can be extracted after the ionization by the electric field and reach the detector.

The way how to extract from this information the kinetic energy distribution is described in detail in refs 17 and 46. The key is a complete simulation of the ongoing process. First, the angular distribution of the photodissociation, the laser polarization, and the kinetic energy E_{kin} are the input parameters. Then the velocity distribution of the molecular beam, the finite interaction volume, the detector dimensions, and the acceleration of the ion trajectories are all accounted for and lead to the calculation of time-of-flight spectra for single kinetic energies. These resulting simulated spectra are then fitted to the measured spectra using a least-squares fit algorithm and the corresponding best fit center-of-mass distributions for the kinetic energy are obtained. We note that, in our experimental arrangement, the detection probability is extremely enhanced at small kinetic energies so that we are in particular sensitive to the caged atoms.[17] The reason is the lower transverse velocity and the larger solid angle compared to faster fragments.

C. Other Observables. We note that, aside from observing the kinetic energy distribution of the H atoms, we have also carried out measurements on the branching ratio of the cross sections $R = \sigma^*/\sigma$ in the two spin−orbit states and the angular distribution of the photofragments $I(\theta) = \text{const}(1 + \beta P_2(\cos\theta))$ by changing the laser polarization. For a prompt dissociation with no perturbation by rotations $\beta = -1$ refers to a perpendicular and $\beta = +2$ to a parallel transition.[46]

III. Theoretical Methods

The measurements how detailed they might be need to be accompanied by calculation for a reasonable and sound interpretation. On the other hand, the calculations have to be approximative for such large systems so that an experimental check is quite worthwhile. Thus experiment and theory rely on each other in this complex dynamics of molecules in large clusters. The method of choice for calculating the dissociation and recombination dynamics is a variant of the "surface hopping" method.[12,14] The nuclei are propagated classically on one of the adiabatic potential surfaces. Electronic transitions are described by the time-dependent Schrödinger equation. When the criterion for a hopping is satisfied, the nuclei switch suddenly to the other potential surface and continue to move classically. We will discuss some of the important features and input data in different calculations separately:

A. Potential Surfaces. As was already mentioned, the ground state is usually very well-known from the three-body hydrogen halide−rare gas potentials based on calculations and spectroscopy.[21−26] The excited states interactions are often calculated using the DIM (diatomics-in-molecule) method.[12,14] These are 12 potentials originating from the s-orbital of H and the p-orbital of the halide atoms. The DIM electronic Hamiltonian that contains also the spin−orbit interaction is diagonalized "on the fly" at each point of the atomic trajectories. The calculation of the nonadiabatic couplings of all potentials is certainly necessary for complicated coupling cases and for recombination. In some cases the dissociation of the monomer proceeds mainly over one or two states. In the case of the hydrogen halides usually the $^1\Pi_1$ state is populated from the ground state $^1\Sigma_0^+$ in a perpendicular transition leading to ground-state atoms X. The excited-state X* is reached by different mechanism depending on the spin−orbit coupling. For HCl the initially excited $^1\Pi_1$ state couples mainly to the $^3\Sigma_1^+$ state and, to a lesser extent, to the $^3\Pi_0$ state that lead to Cl*.[65,66] For HI the $^3\Pi_0$ state is directly populated in a parallel transition giving I*.[67−70] HBr is an intermediate case. For smaller wavelengths the first and for larger wavelengths the second mechanism operates.[71,72] Thus HI would be a typical candidate for a simplified two state calculation, if only the pure dissociation is required. For the rest of the potential surface usually pair potentials are applied. Here the hydrogen−rare gas potential is quite critical, since it determines the efficiency of caging of the H atoms in the repulsive range above 1 eV. In recent ab initio calculations it was demonstrated that a reliable potential is much less repulsive[15] than a series of empirical potentials obtained from low energy molecular beam data[73,74] that are apparently not sensitive to this part of the potential.

B. Initial State Distribution. A critical issue is the preparation of the initial state. This is comparatively easy for the embedded case. Here the molecule is assumed to rotate freely in the middle of the icosahedral rare gas cluster with an isotropic distribution of the H atom around the X atom.[12] For a quantum treatment of the rotation we refer to Ref. 15. For the surface case, we have to take into account the different structural isomers. There are essentially three possibilities.[14,17] (1) The HX is adsorbed on the smooth part of the Rg_n cluster, for example, on the surface of a closed shell Ar_{55}. (2) The HX replaces one Rg atom in the outer shell of the cluster. This would lead in our example to HX-Ar_{54}. Actually such a structure is often a local or even the global minimum of the potential energy surface with large barriers to the other minima. In the case of HCl−Ar_{54} the H atom is a little bit tilted away from the Cl center-of-mass axis.[17] (3) There is still the possibility that the HX molecules penetrates further into the second shell of the cluster. This has to be checked, at best, by molecular dynamics simulations.[56] It depends strongly on the size and the attraction of the HX molecule and the cluster and has been discussed in section II.

After having fixed the structure, a normal-mode analysis is carried out. On the basis of the harmonic oscillator wave function, Wigner distributions are taken to get the initial ensembles of positions and momenta for the further calculation of the trajectories. A variant of this method that accounts more on the pure quantum nature of the initial state is to treat the cage modes as decoupled harmonic oscillators but the vibration and the libration (rotation) of the HX molecules fully quantum mechanically.[7]

Thus we have a large variety of options in the calculations starting from different positions of the molecule in and on the cluster, treating the vibrational wave function of the H atom motion fully quantum-mechanically or as harmonic oscillator, and selecting a few potentials or applying the full coupling of all 12 potential surfaces by nonadiabatic transitions.

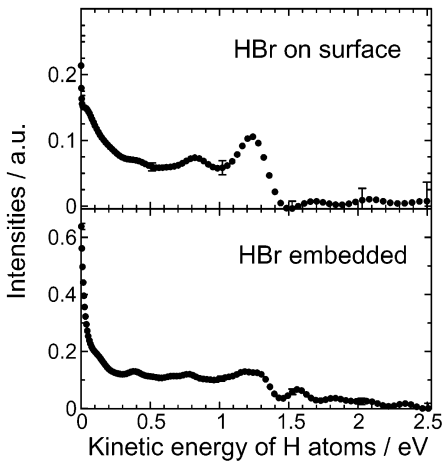

Figure 5. Measured kinetic energy distributions of H atoms from the dissociation at 243 nm. Upper part: HBr molecules on the surface of Ar_n clusters of the averaged size $\langle n \rangle$=97. Lower part: HBr molecules embedded inside of Ar_n clusters of the averaged size $\langle n \rangle$=115.

IV. HBr and HI Molecules on and in Rare Gas Clusters

Before we start to present the results, let us shortly discuss what type of probes the molecules HBr and HI are after the photodissociation with laser light at 243 nm. For HBr, the fraction of 0.8 decays to the ground state after a perpendicular transition so that the kinetic energy of the corresponding H atoms is 1.3 eV.[46,72] The fraction of 0.2 H atoms that correlates with the excited spin−orbit state of Br* has a kinetic energy of 0.9 eV after a parallel transition. The corresponding numbers for HI are 2.0 and 1.0 eV with an equal population in both channels. The bare molecules would therefore produced very narrow kinetic energy distributions of the H atom that peak at exactly these positions with the mentioned amplitudes. We note that with a laser polarization of 90 °, which is used in most of the experiments presented here, mainly, the ground state is populated.

A. Surface and Bulk States of HBr−Ar_n. We will start the presentation of the results with a case study of surface and bulk states. By applying the methods described in detail in section II, we have measured the kinetic energy distribution of HBr molecules that are either adsorbed at the surface of an Ar_n cluster with $\langle n \rangle = 97$ or embedded in a cluster with $\langle n \rangle = 115$. The results are shown in Figure 5.[17] In the surface case, we observe a large contribution at 1.3 eV with a smaller peak at 0.9 eV and a peak with a larger intensity at zero kinetic energy. The former peaks are an indication of the direct cage exit and a reflection of the population in the two spin−orbit states of Br. The latter one is caused by those H atoms which are caged by the interaction with the Ar atoms of the cluster and which appear at zero velocity. For energies larger than 1.4 eV, the intensity is within the experimental error zero. In the embedded case, the general pattern is quite different from that obtained for the surface state. The dominating feature is the very narrow peak at $E_{kin} = 0$. It is much larger than the peak at 1.3 eV which marks those H atoms which have undergone a direct cage exit. Another remarkable difference compared with the results for the surface state is the small but clearly detectable intensity observed at larger energies than 1.3 eV. It is attributed to HBr molecules that are internally excited prior to dissociation. The

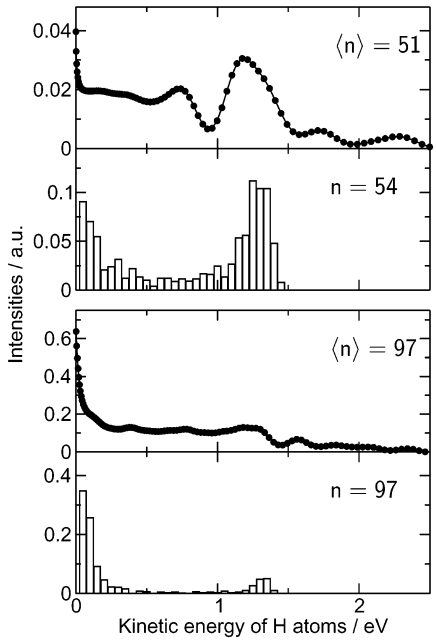

Figure 6. Kinetic energy distribution of H atoms from the photodissociation of embedded HBr molecules in different Ar_n clusters. From top to bottom: measurement $\langle n \rangle = 51$, calculation $n = 54$, measurement $\langle n \rangle = 97$, and calculation $n = 97$.

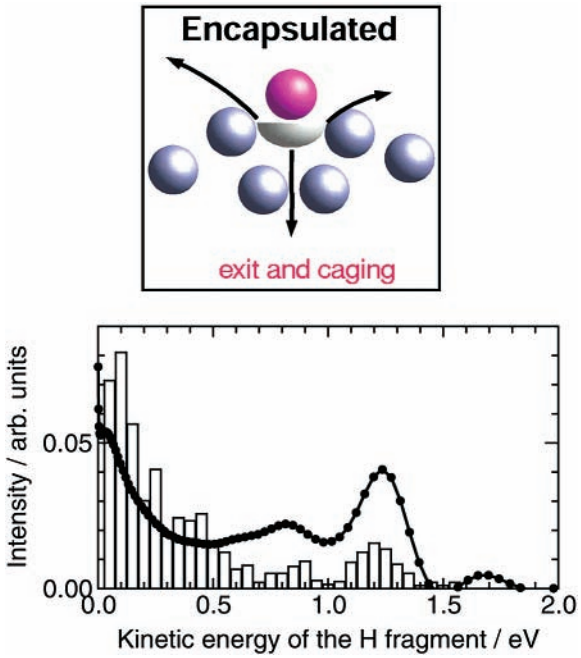

Figure 7. Kinetic energy distribution of H atoms from the photodissociation of surface HBr on Ar_n clusters with $\langle n \rangle = 97$. Points: measurements. Bars: calculations for the encapsulated case that is visualized as cartoon on the upper part.

low intensity of the cage exit peak of H atoms coming from the center of a two and a half shell icosahedron cluster is an expected result. But the relatively large probability of cage exit H atoms starting from the surface of such a cluster comes as a surprise, since the H atoms have to cross the whole cluster.[14]

Now let us look at the size dependence of these results. We investigated HBr clusters on the surface of Ar_n clusters between $\langle n \rangle = 69$ and 139.[75] Their kinetic energy distribution is, within the experimental error, identical to that shown in Figure 5. Thus the results do not depend on the size of the cluster. The same conclusions have been drawn for HI on Xe_n clusters in the size range between $\langle n \rangle = 110$ and 830.[75,76] In contrast, we found for the bulk state, a very strong dependence on the cluster size. In Figure 6 the measurements of the kinetic energy distributions of H atoms coming from the inside of Ar_n clusters with $\langle n \rangle = 51$ and $\langle n \rangle = 97$ are compared. By removing half of the outer shell, the amount of caged atoms drops appreciably and reaches the number of cage exit events. Exactly this behavior has been predicted in a recent calculation by the group of Jungwirth for the same systems.[7] Their results are also displayed in Figure 6. The agreement between experiment and theory is quite close. The main features including the important intensities at $\Delta E = 0.0$ and 1.3 eV are well reproduced although the calculations are carried out for a single size, while the experiments generate clusters with a certain size distribution. The deviations in the 0.4 to 1.0 eV range might be traced back to this effect. The calculations were performed for freely rotating HBr molecules in the central position of the cluster using the formalism described in section III, namely, the quantum dynamical preparation of the initial state and the transition to the important electronic states. Therefore the recombination to internally excited HBr molecules that is observed for energies larger than 1.4 eV is not accounted for.

Given this success, it is also worthwhile to compare the results for the surface case. This is depicted in Figure 7. Again, the calculation is able to reproduce the peaks at zero energy and 1.3 eV and the right trends of their intensities. In addition, the calculations for the argon cluster sizes $n = 54$, 97, and 146 demonstrate that there is only a marginal difference in the kinetic energy distributions, in complete agreement with the measurements.[7] This very convincing agreement allows us to trace back the reason for the relatively large cage exit contribution. In the theoretical work, the initial state is calculated quantum mechanically by the librational motion. This leads, because of the low mass of hydrogen, to a large amplitude motion with a finite probability for escape from the cluster. This is also shown pictorially in the upper part of Figure 7. The further ingredients of the calculation, the surface hopping with the coupling of the main potential surfaces and the use of the new repulsive H−Ar potential are apparently realistic enough to account for this agreement.

There is still a minor difference left in the intensity of the cage exit peaks. Here a rationalization could be invoked that the experimental structures for a given cluster size are probably not unique. As discussed above, in the calculations we have considered surface structures in which the HBr molecule replaces one argon from the outer solvation shell (encapsulated). Another possibility is to deposit HBr on the surface of a cluster with all solvation layers filled (smooth), instead of replacing one of the argon atoms. The calculations of Gerber and Niv for $HCl-Ar_{55}$ show that, in such a case, the component corresponding to fast hydrogen atoms dominates.[17] There is, however, no experimental evidence for this explanation. In fact, the most recent molecular dynamics simulations show that HBr partly penetrates into the second shell,[57] and that from this position it is relatively easy to leave the cluster,[58] since the constraint of the encapsulated site is lifted and about half of the H atoms have to penetrate one shell only. By adding this contribution, nearly complete agreement with the experimnet was obtained.

We can conclude that the good agreement between theory and experiment for both embedded and surface isomers not only indicates the quantitative predictive power of the calculation, but also confirms that the experimental concepts for the production of these clusters are quite reliable.

There is only one experimental part left that deserves further explanations, the weak intensity tail in the embedded case that

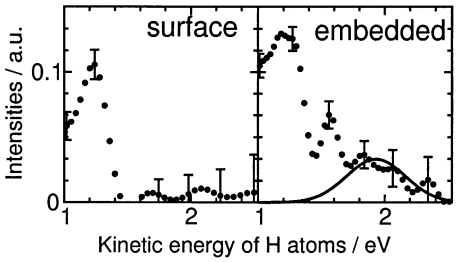

Figure 8. Enlarged part of the distributions of Figure 5 for energies larger than 1 eV in order to visualize the contribution from internally excited, recombined HBr. The solid curve is fitted to the data.

corresponds to internally excited HBr molecules. The result is presented in Figure 8 in an enlarged version of Figure 5. The energy distribution consists of a broad peak with a maximum at 1.9 (0.6) eV that disappears at 2.4 (1.1) eV and a smaller peak at 1.6 (0.3) eV. The numbers in parentheses give the energy content measured from the value of the direct cage exit. The explanation is that HBr molecules that underwent photodissociation have, in part of the cases, recombined. We suggest that some of these recombined molecules have absorbed a second photon before they underwent complete vibrational relaxation. This produces the "superhot" H atoms. In the simulations on HCl embedded inside Ar_{54} several trajectories corresponding to such events were computed.[17] Following the recombination onto the ground state (which takes place 20−60 fs after the photoexcitation) the molecule departs from the cluster, while the H atom vigorously rotates and vibrates around the Cl atom, and the cluster remains only slightly disturbed. At this point, according to the simulation, the second photon (of the same energy as the first one) was absorbed and the molecule finally separates. Most of the energy should remain in rotation, since pure vibrational relaxation is too slow for the absorption of the second photon. This is in agreement with the experimental findings, if we interpret the broad peak as rotation.

B. Dependence on Host Cluster Mass. After having established the complete interpretation of the data for HBr−Ar_n, it is interesting to look at the kinetic energy distributions of the H atoms coming from HBr molecules on the surface of other rare gas clusters. The results are shown in Figure 9 for Ne_n, Ar_n, Kr_n, and Xe_n in the size range from $\langle n \rangle = 124$ to 143.[75] All four distributions exhibit the expected double peak structure around 1.3 and 0.9 eV that is the indication of the direct cage exit and a reflection of the population in the two spin−orbit states of Br. In addition, a further peak appears at zero or small kinetic energies, which is caused by H atoms which are completely caged by the interaction with the rare gas cluster atoms. This peak, however, depends strongly on the rare gas. For neon it peaks at zero energy with a very narrow distribution and an intensity ratio to the peak at the direct cage exit $R_c = I(E_0)/I(E_e) = 10.7$. For argon, the peak position is still at zero energy, but the distribution becomes broader with $R_c = 2.2$. For krypton and xenon this trend is continued. The distribution is still broad and the maximum is shifted to 0.05 and 0.4 eV, respectively, with intensity ratios $R_c = 1.0$ and $R_c = 0.7$, respectively. For energies larger than 1.4 eV, the intensity is within the experimental error zero. This general behavior is certainly a reflection of the inability of the rare gas cage to slow the H atoms with increasing mass. The simplest estimation based on central encounters gives an energy transfer $\Delta E/E = 0.18$ for Ne, 0.10 for Ar, 0.05 for Kr, and 0.03 for Xe per collision. This is in line with experiments and calculations of the mobility of H atoms in matrixes in which times for thermalization of 0.4, 0.7, and 1.1 ps were found for Ar, Kr, and Xe, respectively.[77] Calculations of the dissociation process in clusters give about 10 collision for Ar (ref 10) and 50 collisions for Xe (ref 8) to take the energy out of a fast H atom. We note that the cluster is heated in this process and starts to partly evaporate. While the peak of the caged atoms with $\Delta E = 0$ shows the expected behavior, the cage exit peak should be similar for all four rare gases. This is valid for Ar, Kr, and Xe but not for Ne. Here we observe a smaller cage exit probability that is also responsible for the large value of R_c.

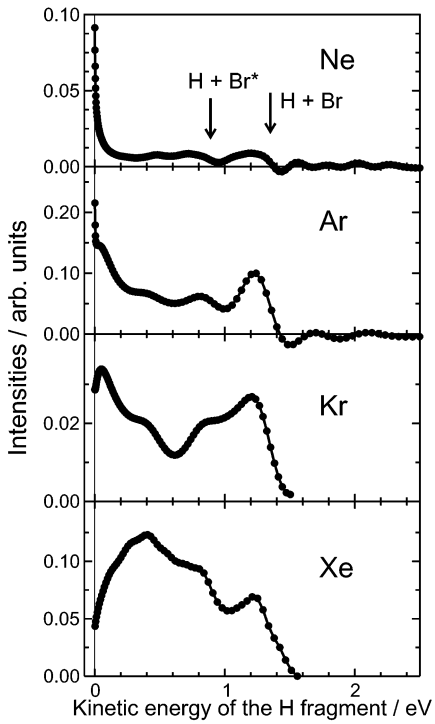

Figure 9. Measured kinetic energy distributions of H atoms from the dissociation at 243 nm in arbitrary units: HBr molecules on the surface of different rare gas clusters Rg_n of the averaged size $\langle n \rangle = 130$. The nominal cage exit energies that are related to the two spin−orbit states of Br are marked.

C. Experiments with HI. As was already mentioned in the beginning of this section, the results for HI should be quite similar, aside from the fact that the kinetic energy available is with 2.0 eV higher than the 1.3 eV of HBr. The results for surface HI molecules on different rare gas host clusters are depicted in Figure 10.[75] They exhibit in fact the expected behavior. The distribution for Ne looks quite similar with a lower ratio $R_c = 5.6$ of caged to cage exit atoms. We also observe the expected decreasing amount of H atoms with zero energy when going from Ne to Xe. The maximum intensity moves already for Kr from 0 to 0.4 eV.

We note here that this general result observed in these measurements is not straightforward, if we consider the behavior of the heterogeneous dimer. While for all HBr−Rg and the HI−Ne complexes the H atom points into the direction of the rare gas atom in the ground state, this is not the case for HI−Ar. In this case the I atom points to the Ar atom and in any dissociation the H atom is not hindered at all.[78−80] In a detailed calculation Slavíček et al. found that this trend of the dimer continues to the trimer.[78] The reason is a trade off between induction forces, caused by the dipole moment of the molecule, that favor the I−H−Ar configuration and increasing dispersion forces that prefer a H−I−Ar configuration. The complete calculation of the librational wave function that is shown in Figure 11 demonstrates that for $HIAr_3$ the H atom points for the first time

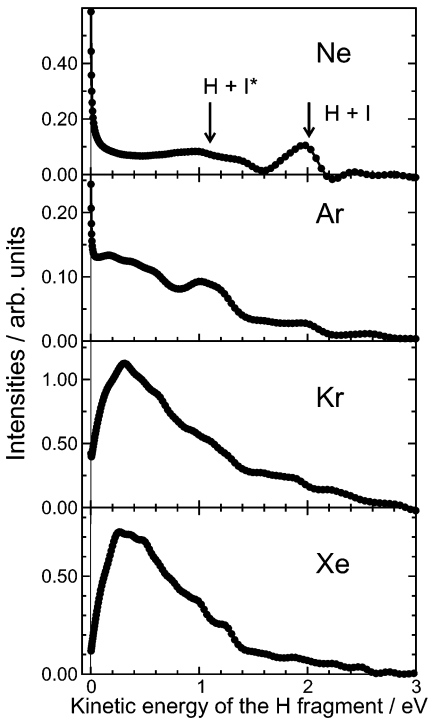

Figure 10. Measured kinetic energy distributions of H atoms from the dissociation at 243 nm in arbitrary units: HI molecules on the surface of different rare gas clusters Rg_n of the averaged size $\langle n \rangle = 130$. The nominal cage exit energies which are related to the two spin−orbit states of I are marked.

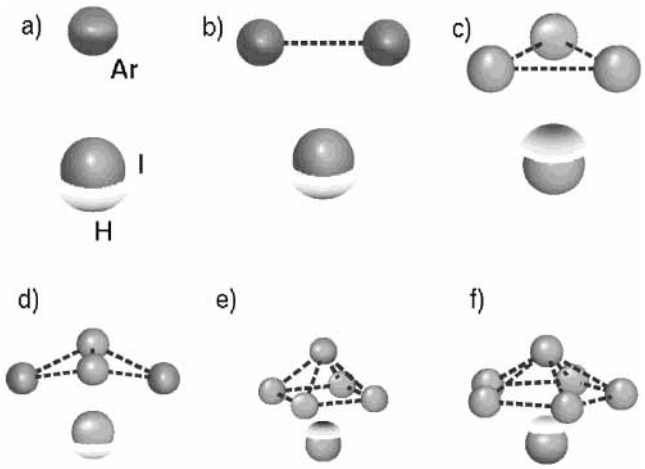

Figure 11. Size dependence of the ground-state librational wave function for HI on Ar_n (n=1−6) from ref 78.

into the direction of the argon atoms. They flip back again for $HIAr_4$, since, in this case, they interact effectively only with two atoms, but stay finally in the direction of the cluster from $HIAr_5$ onward in qualitative agreement with our experimental result for larger clusters presented in Figure 10.

If we compare the results for HBr and HI, we make a surprising discovery concerning the intensity of the cage exit atoms. For HBr this intensity peak is similar for Ar, Kr, Xe but larger than that for Ne. The case of HI exhibits the same similarity for the larger rare gases, but now the intensity is smaller than that for Ne. This conclusion is also valid, if we compare the two groups with each other. The peaks originating from HI−Ar_n, −Kr_n, −Xe_n are smaller than those from HBr−X_n, and for neon clusters, it is just the other way around. Apparently, there are two different mechanisms operating for neon clusters and for the other heavier rare gas clusters.

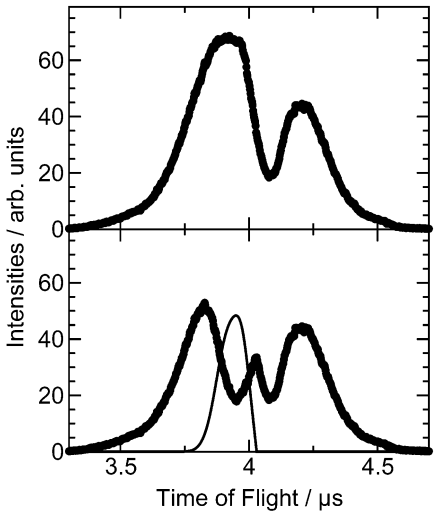

Figure 12. Measured time-of-flight distributions of H atoms from the dissociation of the system HI−Xe_n at 243 nm in arbitrary units for $\langle n \rangle = 830$. Upper part: measured values. Lower part: symmetric (points) and asymmetric (line) part of the spectrum.

Let us first discuss the heavier rare gases. Although more energy is available for HI, the intensity for the cage exit into the ground state is smaller than that for HBr. Initially we thought that the explanation for this behavior is given by the fact that HI is found after the pick-up process in the second shell of the heavier rare gas clusters because of the increasing van der Waals attraction between the molecule and the host cluster atoms.[56] This was indeed confirmed in a recent Molecular Dynamics simulations by Vach.[57] The calculations on the dynamics based on this result, however, show that the exit probability increases in such a case.[58] This is observed for the excited I* state at about 1 eV where it should not be present at a laser polarization of 90 °. We think that this is a clear manifestation of a cluster induced state mixing that was not taken into account in the calculation. Further efforts are needed to clarify this point.

The HI−Ne_n cluster case is definitely different, since here the peak is higher compared with HBr and the other rare gases. Obviously, the HI is sitting in a much less constraint environment than in the heavier rare gases. The simplest and most plausible explanation is that HI and HBr penetrate completely in the pick-up process inside the cluster. This explains the experimental results. For HBr, for instance, less H atoms escape from the inner part than from the first and second shell. In the comparison of HI and HBr in Ne_n the more probable cage exit for HI is caused by the higher kinetic energy. We also note the similarity of the distributions of HBr−Ne_n and the embedded case of HBr−Ar_n (see Figure 6). What is left is to give a reason why this occurs. We suggest that neon clusters in this size range are liquidlike after the capture of an HX molecule. A similar process has been observed recently for Xe−Ne_n clusters.[81] By measuring the fluorescence excitation spectra of these clusters, only bulk states were observed up to cluster sizes of $\langle n \rangle = 200$. From $\langle n \rangle = 300$ onward, also surface sites appear in the spectra. The authors interpret that as a sort of phase transition from solid to liquidlike behavior. We should see similar results and experiments are underway in our laboratory to clarify this point.

V. Experimental Detection of the HXeI Molecule

For one of the investigated systems, HI−Xe_n, and only for this one, we observed a very interesting feature in the time-of-flight spectra that are depicted in Figure 12.[76] The upper part shows the raw data that are characterized by a strong asymmetry

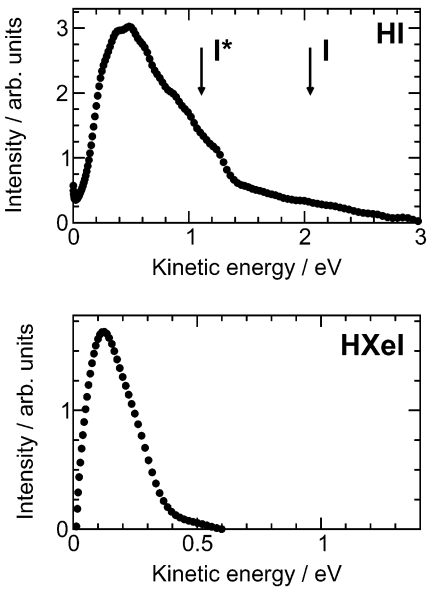

Figure 13. Measured kinetic energy distributions of H atoms from the dissociation at 243 nm in arbitrary units: Upper part: HI molecules on the surface of Xe_n clusters for $\langle n \rangle = 830$. The nominal cage exit energies which are related to the two spin−orbit states of I are marked. Lower part: HXeI molecules originating from a HI−Xe_n cluster with $\langle n \rangle = 830$. Note the reduced energy scale compared to the upper part.

in the intensity. This pronounced asymmetry is a clear indication that part of the intensity originates from dissociation processes of oriented molecules. This feature does not depend on the cluster size. In our experimental arrangement the dissociation of an unoriented molecule, such as HY, always results in a symmetric time-of-flight spectrum of the H atoms as was demonstrated in Figure 4. First the detector sees the H atoms which were emitted in the direction of the detector and finally those H atoms which were initially flying in the opposite direction and then turned around by the weak electric field. This behavior enables us to easily separate the asymmetric part of the spectrum from the rest. We subtract such a distribution from the measured spectrum so that the two symmetric halves of the remaining spectrum give, when transformed to the kinetic energy distribution, identical results. We note that the remaining time-of-flight distributions does not need to be necessarily perfectly identical, since the atoms see different electric field distributions on their way to the detector. The result of such a procedure for the average cluster size $\langle n \rangle = 830$ is displayed in the lower part of Figure 12 where the points represent the symmetric part and the solid line the asymmetric part of the spectrum. Similar results were obtained for the other cluster sizes.

The underlying kinetic energy distributions for the symmetric part of the spectrum are shown in the upper part of Figure 13. The curves obtained for the other cluster sizes are nearly identical. These results are clearly attributed to the dissociation of HI molecules on the surface of Xe_n clusters. The kinetic energy distribution exhibits the typical pattern expected for such an event as was shown in Figure 10. The result for the asymmetric part of the spectrum is depicted in the lower part of Figure 13. Since the second, slower part of the time-of-flight distribution is missing, the detected H atoms have to come from a molecule which is oriented in such a way that the H atom points in the direction of the detector.

We attribute this result to the presence of the molecule HXeI. It belongs to a recently discovered class of rare gas containing hydrides that have been identified in rare gas matrices.[47,82] These molecules of the type HRgY, where Rg is a rare gas and Y a halogen atom, are formed by neutral precursor atoms which, in turn, are obtained by the photodissociation of hydrogen halide HY molecules in solid Rg matrices. They are quite stable molecules with a strong ionic character of the type HRg^+Y^-. A typical example is HXeI which has been thoroughly investigated with respect to the formation and decay mechanisms.[83,84] After the photodissociation, the H atoms are reflected from the cage and recombine with XeI to form HXeI, where the H atom is bound by 0.4 eV at a distance of 1.74 Å.

We will now discuss the reason we are convinced that we have detected oriented HXeI.

(1) The results for the kinetic energy exhibit a distribution which essentially covers the energies from zero to 0.4 eV with a maximum at between 100 and 120 meV. The limiting value of 0.4 eV corresponds exactly to the bonding energy of the H atom to Xe and indicates that no further kinetic energy is gained in the decay process. It probably occurs via electronic predissociation by coupling to other repulsive potential curves.

(2) The *orientation* of HXeI occurs by a very interesting combination of two effects that were recently proposed by Friedrich and Herschbach[85,86] and that were experimentally realized in our apparatus. It is well-known that polar molecules can be oriented in strong electric fields.[87] But the static electric field in our experiment, $E = 4$ eV, is 3 orders of magnitude too small for such a process. The intensity of the laser, however, is high enough to align HXeI by the interaction of the intense nonresonant laser field with the induced anisotropy of the polarization.[88−90] In combination with the weak static electric field the alignment, which still contains two directions, is changed into pure orientation where only one direction is selected, namely the one that the dipole moment points to.

The HXeI molecule has all these properties. First, it has a very large anisotropy of the dipole polarizability $\Delta\alpha$ with respect to the rotational constant B so that it can be easily aligned even in our laser field with the moderate effective intensity $I_l = 1.1 \times 10^{11}$ W/cm^2. Second, HXeI has a large dipole moment $\mu = 6.4$ D, that points into the direction of the H atom. This is exactly the direction where we measured the asymmetry. The two key parameters that determine the possible orientation are[86] $\Delta\omega = 10^{-11}\Delta\alpha(\text{Å}^3)I_l(\text{W cm}^{-2})/B(\text{cm}^{-1})$ and $\omega = 0.0168\mu(D)E(\text{kV/cm})/B(\text{cm}^{-1})$. The first term is reponsible for the alignment and the second one for the Stark effect. $\Delta\alpha$ was estimated from α of the constituents using a relation between α and $\Delta\alpha$ derived from the similar systems I_2 and Br_2. With the data presented in Table 1, we get $\Delta\omega = 225$ and $\omega = 0.016$ for our experimental arrangement. Friedrich calculated the expectation value of the orientation cosine $\langle \cos\theta_s \rangle = 0.97$.[91,92] This value clearly demonstrates that we dissociate indeed nearly completely oriented HXeI molecules. For comparison, the data for HI are presented. The much smaller parameters are not sufficient for any alignment or orientation.

There is, however, a problem that rises from the small electric field. In the present combination of nonresonant laser and static electric fields, pendular states are generated that are superpositions of field-free rotational states.[86] The calculated example corresponds to the ground state with $\tilde{J} = 0$, $M = 0$. Since the energy of the Stark effect is small, the state $\tilde{J} = 1$, $M = 0$ that leads to the wrong orientation with $\langle \cos\theta_s \rangle = -0.97$ can easily be populated in a thermally averaged ensemble. We have, however, to keep in mind that these consideration are obtained for free molecules, while, in our case, HXeI is after formation still embedded in the Xe_n cluster. In fact, recent simulations by Bihary and Gerber demonstrate that HXeI does barely rotate

TABLE 1: Characteristic Data for the Orientation of Different Molecules: Δα Anisotropy of Dipole Polarizabilities, *B* Rotational Constant, *μ* Dipole Moment, ⟨cos θ_s⟩ Orientation Cosine[a]

molecule	Δα/Å^3	B/cm^{-1} [b]	μ/D[c]	ω	$\Delta\omega$	⟨cos θ_s⟩
HXeI	5.5	0.027	6.4	0.016	225	0.97
HI	0.43	6.551	0.45	0.005	0.072	0.002

[a] The dimensionless parameters ω and $\Delta\omega$ are defined in the text. [b] Geometries from ref 47. [c] Reference 47.

with a zero point energy amplitude of the bending motion of less than 2°.[92,93]

(3) Finally, we have to show why we observe this effect only for one system, namely HXeI. There is a trade off between the requirements for the large polarizabilities that are necessary for the alignment and the stability of these molecules that result from large ionic components. The former condition prefers the heavier components, while the latter one is in favor of the lighter components. From the next possible candidates, HXeBr and HKrI, the first one has not yet been measured, and the second one has not been observed, neither in experiment nor in calculations.

We conclude this section by describing again the process of the formation and detection of HXeI in a pictorial way in Figure 14. In the first step HI is photodissociated near the surface of the Xe_n cluster. The H atom moves to the next shell, is backscattered and finally captured by the remaining XeI that did not move after the dissociation because of its heavy mass. Then the HXeI molecule is turned over into the direction of the combined laser and electric field. During this process most of the Xe atoms evaporate. This adiabatic following requires a long laser pulse, under our conditions longer than 5 ns,[94] that is easily fulfilled by our laser system. Finally the molecule HXeI is oriented and dissociated within the same laser pulse.

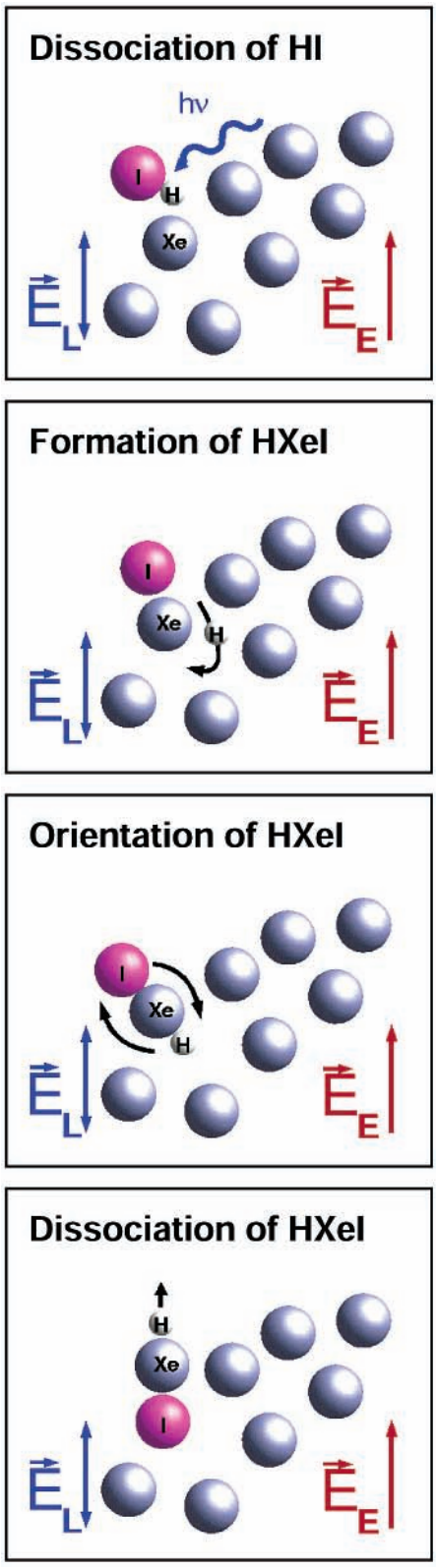

Figure 14. Pictorial view of the production and orientation of HXeI.

VI. HBr_x Complexes in and on Large Ar_n Clusters

The preparation of small complexes adsorbed on the surface or embedded in large Ar_n clusters takes place in the same way as that of single molecules. With the help of the pick-up technique, small complexes of different compositions are generated for different cell pressures. Embedded complexes are produced by expanding a suitable mixture of HBr in argon. They exhibit, aside from the same features as single molecules namely cage exit and caging events, indications of internally excited molecules. These result from collisions of already dissociated, fast H atoms with intact neighbor molecules of the same complex that are subsequently dissociated within the same laser pulse.

$$(HBr)_x + h\nu \rightarrow H + (HBr)_{x-1} + Br \quad (2)$$

$$H + (HBr)_{x-1}H + HBr(J,v)(HBr)_{x-2} \quad (3)$$

$$HBr(J,v)(HBr)_{x-2} + h\nu \rightarrow H' + Br + (HBr)_{x-2} \quad (4)$$

Such events were first observed by Wittig and co-workers[40] and attributed to HI dimers. Later on we measured them for pure HBr clusters with a threshold around $n = 6$.[46] Since the collisions occur in a constraint geometry, it is quite interesting to compare these results with those obtained for isolated H + HX collisions.[95−97] We will discuss the results of the different initial state preparations separately.

A. Embedded Case. The results for $(HBr)_x$ complexes with $\langle x \rangle = 8$ that are completely or partly enclosed in Ar_n clusters with the average size range $\langle n \rangle = 100$ to 12 are depicted in Figure 15.[48] All the kinetic energy distributions are dominated by three peaks starting at 1.3 eV that belong to cage exit H atoms from HBr in $v = 0$, 1, and 2. The remarkable result is the very narrow width of these peaks that indicates a very small rotational excitation. We estimate from the half width at half-maximum $\Delta E = 75$ meV a rotational energy transfer $\Delta J = 8$. Similar results have been obtained in a molecular beam experiment in which fast H atoms collide with HBr.[95] The

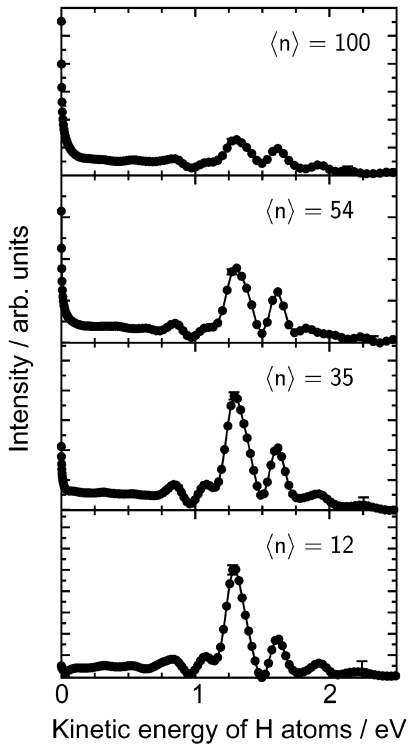

Figure 15. Kinetic energy distributions of the H fragments after 243 nm dissociation of $(HBr)_x$ complexes with $\langle x \rangle = 8$ embedded in Ar_n clusters for the different sizes noted. In the expansion a mixture of 1% HBr in argon was used at different temperatures.

corresponding quasi-classical trajectory calculations carried out for the similar prototype system H + HI clearly indicate that such a result is only obtained for the inelastic collisions, while the exchange reaction H′ + HI → H + H′I is always accompanied by much larger amounts of rotational excitation in the order of $\Delta J = 28$.[97] Thus we conclude that the mechanisms for the vibrational excitation are mainly inelastic collision of the type H + HBr. Although the fast H atoms start from well defined positions when they collide with the other molecules in the cluster, the final result is in agreement with a calculation of the integral cross section which is averaged over all directions. We note that in the different cluster arrangements nearly all directions contribute.

The amount of vibrational excitation that we measure by the ratio of the intensity in $v = 1$ to that in $v = 0$, $R_v = I(v = 1)/I(v = 0)$, decreases from 0.75 to 0.34 for decreasing Ar_n cluster sizes. The measured ratio R_v in the single collision experiment for H + HBr is 0.25,[95] in good agreement with the results 0.22 obtained for neat clusters.[46] Since this value is only slowly approached for decreasing Ar_n cluster size in the present experiments, we have to explain why the presence of the Ar_n clusters increases the amount of vibrational excitation. A plausible explanation is the reduced velocity of the colliding H atoms after they have been backscattered from the Ar cage. This probability increases the larger the argon cluster is. The test calculations for H + HI using the realistic DIM-3C surface indeed show that the cross section for vibrational excitation increases by about a factor of 2 when the collision energy is lowered from 1.6 to 0.7 eV (see Table 1 of ref 97).

A further remarkable results is the large variation of the fraction of caged H atoms, measured by the ratio of intensities at $E_{kin} = 0$ and $E_{kin} = E_e$, the energy at the unperturbed cage exit $R_c = I(E_0)/I(E_e)$. It varies from 4.6 for $\langle n \rangle = 100$ to 0.1 for $\langle n \rangle = 12$. By choosing the right size of the surrounding Ar_n clusters, by varying the source temperature and the mixture, the amount of caged H atoms can be shifted to any size wanted. This is also an interesting environment for promoting reactions, if we enclose two different species. Similar ideas have already been realized experimentally.[98]

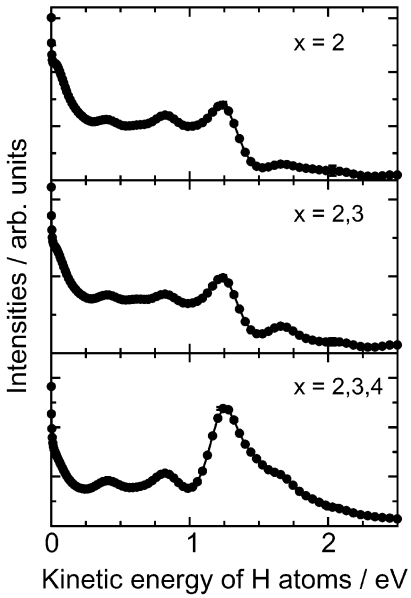

Figure 16. Kinetic energy distributions of the H fragment after 243 nm dissociation of $(HBr)_x$ complexes on the surface of Ar_n clusters for different pressures. The contributing x values are specified.

B. Surface Case. The kinetic energy distributions for small $(HBr)_x$ complexes adsorbed on the surface of Ar_n with $\langle n \rangle = 139$ are shown in Figure 16.[48] The distributions are again dominated by a peak at $\Delta E = 0$, the caged atoms, and a peak at 1.3 eV that consists of atoms directly leaving the cage. In contrast to the results for the embedded case, the fraction of caged atoms is about the same and the peaks that are caused by vibrationally excited HBr molecules are smeared. Here obviously an appreciable amount of rotational excitation is present.

The composition of the clusters on the surface is well-known from the pick-up production process. The monomer fraction decreases from 0.55 to 0.23, the dimer fraction stays constant at about 0.30, and the trimer fraction increases from 0.12 to 0.28 as does the tetramer fraction from 0.03 to 0.28. Since the amount of caged atoms is about the same, we conclude that the escape probability of the monomers and the small clusters are quite similar. As for the internal excitation, we have to distinguish between dimers and tetramers, which lead in the upper and the lower part to very broad distributions, while the trimers which appear first in the middle part, exhibit a more structured curve. A possible explanation for this behavior is as follows. In the probable configuration of the $(HBr)_2$ dimer on the argon surface, the free HBr molecule is pointing with the H-end to the cluster surface, while the hydrogen bonded molecule points with its H atom in the direction of the Br atom of the first one as is shown pictorially in Figure 17. This configuration already explains why the vibrational excitation is accompanied with a larger amount of rotational excitation than is observed for embedded clusters. The reason can be rationalized by the constrained geometry under which the H atom collides with the Br part of the HBr molecule. Aside from the pictorial understanding of transferring a reasonable torque to the molecule, such a behavior has also been observed in quasi-classical trajectory studies of the very similar system H + HI at comparable collision energies.[97] In fact, for the more realistic

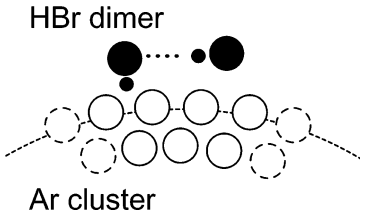

Figure 17. Schematic structure of the $(HBr)_2$ dimer on the surface of the Ar_n cluster.

anisotropic DIM-3C surface, the amount of inelastic energy transfer caused by the H − HBr collision increases by nearly a factor of 2 when going from the collinear to the perpendicular approach which is realized in the present arrangement (see Figure 12B of Ref. 97). The inelastic collisions which occur within the trimer resemble apparently more those found in the embedded case, while the nearly perpendicular arrangement of the tetramer resembles more the dimer than the trimer that shows a much higher escape probability than the other two.

C. Pure $(HBr)_x$ Clusters. We already discussed part of the results that we have obtained for the average size $\langle x \rangle = 8$[46] in section VI.A as the limiting case for similar complexes embedded in Ar_n clusters. The general pattern of the kinetic energy distribution of the H atoms resembles that observed for $\langle n \rangle = 12$. But the absence of only 12 argon atoms leads still to a lower vibrational excitation, expressed by $R_v = 0.22$, and a lower cage effect, expressed by $R_c = 0.03$. The corresponding values for the mixed cluster $(HBr_x)-Ar_n$ with $\langle x \rangle = 8$ and $\langle n \rangle = 12$ are $R_v = 0.34$ and $R_c = 0.1$, respectively. In addition to these results, we measured for the pure clusters the branching ratio of the spin−orbit states and the angular dependence of the products. The branching ratio for the cage exit events is with $R = 0.17$ for 193 nm and $R = 0.18$ for 243 nm nearly the same as was found for the monomer. Similar results have been found for the β parameters (see Sec. II.C). Despite of the same magnitude of the branching ratios, the processes that are operating for the two wavelengths are quite different. At 243 nm, we observed with $\beta^* = 2.00$ a parallel transitions leading to the excited state and with $\beta = -0.88$ a perpendicular transition for the ground state. The results for 193 nm are $\beta^* = -0.20$ and $\beta = -0.80$, respectively. Again the deviations with respect to the monomer results are small. We conclude that the cluster environment of a small, pure $(HBr)_x$ cluster does not really change the dynamics of the cage exit processes. The very small amount of caged atom at 243 nm exhibits, as expected an isotropic angular dependence. At 193 nm, no such events were observed.[46]

VII. Summary and Future Prospects

This review has touched on several new developments in the photodissociation of single molecules that are placed close to the surface or inside large clusters. While the theoretical studies on this subject had already reached a high level of quality in recent years, experimental methods for neutral systems and other than small complexes are just available.

As case studies the halogen halide molecules HBr and HI are investigated in the interaction with the rare gas clusters Ne_n, Ar_n, Kr_n, and Xe_n in the size range from $\langle n \rangle = 50$ to 830. The initial surface states are generated by applying the pick-up technique and the embedded states by the usual co-expansion. By measuring the kinetic energy of the H product atom, detailed information on the direct cage exit and the complete caging with subsequent recombination is obtained. In a combined effort of theoretical calculations and the detailed measurements for

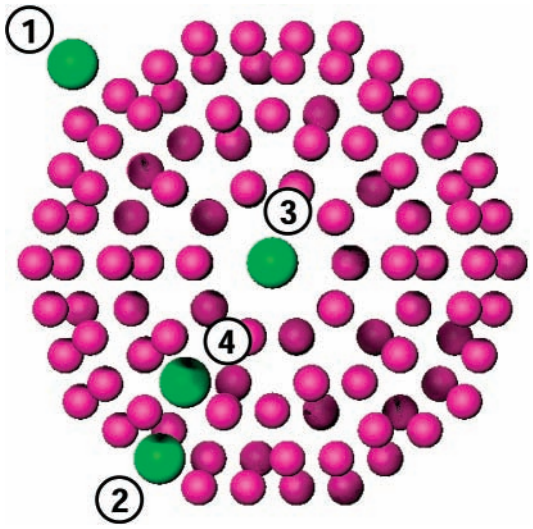

Figure 18. Schematic positions of the halogen halide molecule (black) in or on a rare gas cluster of $n = 147$ with three filled shells.

surface and embedded states of $HBr-Ar_n$ in the size range from $\langle n \rangle = 60$ to 140 good agreement is obtained. To reach this agreement, the calculations, that were mainly based on the surface hopping model, accounted for the correct quantum description of the initial state and used the most recent H−Ar interaction potential. On the basis of this nice agreement between measurements and theoretical predictions, a very detailed picture emerges how diatomic molecules behave when they are photodissociated.

We will discuss the results with respect to the probability for cage exit and caging of the different sites that are depicted pictorially in Figure 18. (1) Molecules that are absorbed on the surface of a more or less closed shell rare gas cluster exhibit a large cage exit probability, mainly because of the large amplitude motion of the H atoms. This case has been observed in a calculation for $HCl-Ar_{55}$,[17] but up to now we did not found any experimental evidence for this case. (2) Here the molecule is encapsulated in the first shell of the cluster where it replaces one of the rare gas atoms, the ideal surface position. Because of the attractive forces, the H atom is in contraint position between rare gas atoms and the probability to be caged is larger than for the cage exit. In fact, the latter results only from the large amplitude motion of the H atom. Typical examples are HBr molecules on the surface of Ar_n, Kr_n, and Xe_n clusters, produced by the pick-up technique. This behavior does not depend on the cluster size as was observed both in experiment and calculations. (3) This is the typical embedded case. In contrast to the surface case (2) the H atom is not restricted in its direction when it tries to get out of the cage. A typical example is $HBr-Ar_n$ produced by co-expansion. Here the fraction of caged to cage exit atoms depends sensitively on the size of the host cluster being about equal for $\langle n \rangle = 54$ and approaching zero for $\langle n \rangle = 140$. This trend has been verified in the experiment. The experimental results also demonstrated that HBr and HI on Ne_n clusters behave in the same way so that we suggest that in this case the molecules go completely inside the cluster because they are liquidlike. Position (4) in the second shell is a very interesting case. Here the H atoms are again freely rotating as in case (3) but now a fraction has to cross one shell only with a high exit probability accompanied by another fraction in the backward direction with low exit probability. For clusters in the size range of $n = 100$ the cage exit probabiliy is larger than for the embedded case. Examples are HI, and partly also HBr molecules, generated by pick-up on the rare

gas clusters Ar_n, Kr_n, and Xe_n. For HI this effect is, admittedly, more pronounced for the excited I* than for the ground state. We note that in cases where we were able to compare the ability of the host cluster to promote the cage effect, it increases when going from Xe to Ne, certainly an effect of the mass to slow the light H atoms.

In the photodissociation of $HI-Xe_n$ we observed also H atoms coming from the dissociation of oriented HXeI molecules. They belong to a recently found class of ionically bound molecules that have been identified in matrices. In our experimental arrangement the combination of the strong laser and the weak electric field lead to the orientation of the molecule that does not rotate in the Xe environment when it is formed.

Finally, we were also able to place small complexes of $(HBr)_x$ on the surface and inside Ar_n clusters of different sizes. In these experiments the most remarkable result is the internal excitation of the single HBr molecules by the fast H atoms of already dissociated neighbor molecules. Depending on the constraint of the complexes we observe either pure vibrational or dominating rotational excitations. In the embedded case the rare gas cluster works as a sort of cage for the dynamical process so that such an arrangement would also be an effective environment for a chemical reaction.

In looking to the future, several experiments are in need for completing the results already obtained. For HI, experiments for different laser polarization and the corresponding theoretical treatment are in progress. Also the questions of how many shells are necessary to prevent the H atoms completely from leaving the cage has to be answered experimentally. In addition, the suggestion that small Ne_n are liquid has to be verified in detailed experiments. The orientation of HXeI can be proved experimentally by changing the direction of the electric field. Both experiments are being under way in our laboratory.

The next experimental step will be the change of the dissociation wavelength. Going from 243 to 193 nm, opens up the possibility to work in the maximum of the absorption curve for HBr and to access the dissociation of HCl interacting with all the rare gases. For these systems most of the calculations have been carried out so that additional direct comparisons will become feasible. In general, one should note that the experimental method presented here is not at all restricted to halogen halides and rare gas clusters. In this sense, it would be quite interesting to investigate the dissociation of HCl and HBr on $(H_2O)_n$ clusters. Here the transition to charge separated states should occur and the present experimental method should throw new light on these important reactions. The extension to other molecules that play a crucial role in atmospheric chemistry on ice surfaces is straightforward. By decreasing the wavelength again and using 157 nm, the new field of experiments with water in different cluster environments is made accessible. We stress again that the main progress in this field is the concerted action of experiment and theory, since one without the other would only lead to experimental results that are difficult to interpret and calculations whose exact meaning is difficult to judge.

Acknowledgment. This work has been supported by the Deutsche Forschungsgemeinschaft in SFB 357 and the DAAD-NSF exchange program. The author gratefully acknowledges the crucial contributions from his former and present students Dr. C. Frischkorn, Dr. R. Baumfalk, N. H. Nahler, and the cooperation with Prof. L. Hüwel, Wesleyan, in this work. He is also quite grateful for the very fruitful cooperations in the interpretation of the data with Prof. R. B. Gerber, Dr. M. Niv, and Z. Bihary, Jerusalem and Irvine, Prof. P. Jungwirth and P. Slavíček, Prague, Dr. B. Friedrich, Harvard, and Dr. H. Vach, Palaiseau. The author finally thanks N.H. Nahler for many helpful discussions and his valuable assistance in preparing the figures.

References and Notes

(1) Franck, J.; Rabinovitsch, E. *Trans. Faraay Soc.* **1934**, *30*, 120.
(2) Apkarian, V. A.; Schwentner, N. *Chem. Rev.* **1999**, *99*, 1481.
(3) Harris, A. L.; Brown, J. K.; Harris, C. B. *Annu. Rev. Phys. Chem.* **1988**, *39*, 341.
(4) Schröder, J.; Troe, J. *Annu. Rev. Phys. Chem.* **1987**, *38*, 163.
(5) Fleming, G. R. In *Chemical Application of Ultrafast Spectroscopy*; Oxford University Press: New York, 1986.
(6) Gerber, R. B.; McCoy, A. B.; Garcıa-Vela, A. *Annu. Rev. Phys. Chem.* **1994**, *45*, 275.
(7) Slavíček, P.; Žďánská, P.; Jungwirth, P.; Baumfalk, R.; Buck, U. *J. Phys. Chem.* **2000**, *104*, 7793.
(8) Alimi, R.; Gerber, R. B. *Phys. Rev. Lett.* **1990**, *64*, 1453.
(9) García-Vela, A.; Gerber, R. B.; Buck, U. *J. Phys. Chem.* **1994**, *98*, 3518.
(10) Schröder, T.; Schinke, R.; Liu, S.; Bačić, Z.; Moskowitz, J. W. *J. Chem. Phys.* **1995**, *103*, 9228.
(11) Narevicius, E.; Neuhauser, D.; Korsch, H. J.; Moiseyev, N. *Chem. Phys. Lett.* **1997**, *276*, 250.
(12) Niv, M.; Krylov, A. I.; Gerber, R. B. *Faraday Discuss. Chem. Soc.* **1997**, *108*, 243.
(13) García-Vela, A. *J. Chem. Phys.* **1998**, *108*, 5755.
(14) Niv, M. Y.; Krylov, A. I.; Gerber, R. B.; Buck, U. *J. Chem. Phys.* **1999**, *110*, 11047.
(15) Žďánská, P.; Schmidt, B.; Jungwirth, P. *J. Chem. Phys.* **1999**, *110*, 6246.
(16) Žďánská, P.; Slavíček, P.; Jungwirth, P. *J. Chem. Phys.* **2000**, *112*, 10761.
(17) Baumfalk, R.; Nahler, N. H.; Buck, U.; Niv, M. Y.; Gerber, R. B. *J. Chem. Phys.* **2000**, *113*, 329.
(18) Monnerville, M.; Pouilly, B. *Chem. Phys. Lett.* **1998**, *294*, 473.
(19) Schmidt, B. *Chem. Phys. Lett.* **1999**, *301*, 207.
(20) Hutson, J. M. *J. Chem. Phys.* **1988**, *89*, 4550.
(21) McIntosh, A.; Wang, Z.; Castillo-Chara, J.; Lucchese, R. R.; Bevan, J. W.; Suenram, R. D.; Legon, A. C. *J. Chem. Phys.* **1999**, *111*, 5764.
(22) Hutson, J. M. *J. Phys. Chem.* **1992**, *96*, 4237.
(23) Hutson, J. M. *J. Chem. Phys.* **1992**, *96*, 6752.
(24) Meuwly, M.; Hutson, J. M. *J. Chem. Phys.* **1999**, *110*, 8338.
(25) Hutson, J. M. *J. Chem. Phys.* **1989**, *91*, 4448.
(26) Hutson, J. M. *J. Chem. Phys.* **1989**, *91*, 4455.
(27) Anderson, D. T.; Davis, S.; Nesbitt, D. J. *J. Chem. Phys.* **1997**, *107*, 1115.
(28) Nadal, M. E.; Kleiber, P. D.; Lineberger, W. C. *J. Chem. Phys.* **1996**, *105*, 504.
(29) Nandi, S.; Sanov, A.; Delaney, N.; Faeder, J.; Parson, R.; Lineberger, W. C. *J. Phys. Chem.* **1998**, *102*, 8827.
(30) Kades, E.; Rösslein, M.; Brühlmann, U.; Huber, J. R. *J. Phys. Chem.* **1993**, *97*, 989.
(31) Bergmann, K.; Huber, J. R. *J. Phys. Chem. A* **1997**, *101*, 259.
(32) Kades, E.; Rösslein, M.; Huber, J. R. *J. Phys. Chem.* **1994**, *98*, 13556.
(33) Fan, Y. B.; Donaldson, D. J. *J. Chem. Phys.* **1993**, *97*, 989.
(34) Syage, J. A. *Chem. Phys.* **1996**, *207*, 411.
(35) Fenner, K.; Furlan, A.; Huber, J. R. *J. Phys. Chem. A* **1997**, *101*, 5736.
(36) Flesch, R.; Wassermann, B.; Rothmund, B.; Rühl, D. *J. Phys. Chem.* **1994**, *98*, 6263.
(37) Kreher, C.; Carter, R.; Huber, J. R. *J. Chem. Phys.* **1999**, *110*, 3309.
(38) Li, Q.; Huber, J. R. *Chem. Phys. Lett.* **2001**, *345*, 415.
(39) Segall, J.; Wen, Y.; Singer, R.; Wittig, C.; García-Vela, A.; Gerber, R. B. *Chem. Phys. Lett.* **1993**, *207*, 504.
(40) Zhang, J.; Dulligan, M.; Segall, J.; Wen, Y.; Wittig, C. *J. Phys. Chem.* **1995**, *99*, 13680.
(41) Liu, K.; Kolessov, A.; Partin, J. W.; Brezel, I.; Wittig, C. *Chem. Phys. Lett.* **1999**, *299*, 374.
(42) Young, M. A. *J. Chem. Phys.* **1995**, *102*, 7925.
(43) Baumfalk, R.; Buck, U.; Frischkorn, C.; Gandhi, S. R.; Lauenstein, C. *Ber. Bunsen-Ges. Phys. Chem.* **1997**, *101*, 606.
(44) Baumfalk, R.; Buck, U.; Frischkorn, C.; Gandhi, S. R.; Lauenstein, C. *Chem. Phys. Lett.* **1997**, *269*, 321.
(45) Buck, U.; Meyer, H. *J. Chem. Phys.* **1986**, *84*, 4854.
(46) Baumfalk, R.; Buck, U.; Frischkorn, C.; Nahler, N. H.; Hüwel, L. *J. Chem. Phys.* **1999**, *111*, 2595.
(47) Pettersson, M.; Lundell, J.; Räsänen, M. *Eur. J. Inorg. Chem.* **1999**, 729.

(48) Baumfalk, R.; Nahler, N. H.; Buck, U. *Phys. Chem. Chem. Phys.* **2001**, *3*, 2372.
(49) Schütte, S.; Buck, U. *Int. J. Mass Spectrosc.* **2002**. In press.
(50) Karnbach, R.; Joppien, M.; Stapelfeldt, J.; Wörner, J.; Möller, T. *Rev. Sci. Instrum.* **1993**, *64*, 2838.
(51) Hagena, O. F. *Surf. Sci.* **1981**, *106*, 101.
(52) Hagena, O. F. *Rev. Sci. Instrum.* **1992**, *63*, 2374.
(53) Buck, U.; Krohne, R. *J. Chem. Phys.* **1996**, *105*, 5408.
(54) Gough, T. E.; Mengel, M.; Rowntree, P. A.; Scoles, G. *J. Chem. Phys.* **1985**, *83*, 4958.
(55) Behrens, M.; Fröchtenicht, R.; Hartmann, M.; Siebers, J. G.; Buck, U. *J. Chem. Phys.* **1999**, *111*, 2436.
(56) Vach, H. *J. Chem. Phys.* **1999**, *111*, 3536.
(57) Vach, H. 2002. Unpublished results.
(58) Nahler, N. H.; Buck, U.; Vach, H.; Slavíček, P.; Jungwirth, P. *Chem. Phys.* **2002**. In press.
(59) Ashfold, M. N. R.; I. R. Lambert, D. H. M.; Morley, G. P.; Western, C. M. *J. Phys. Chem.* **1992**, *96*, 2938.
(60) Maul, C.; Gericke, K.-H. *J. Phys. Chem. A* **2000**, *104*, 2531.
(61) Chandler, D. W.; Houston, P. L. *J. Chem. Phys.* **1987**, *87*, 1445.
(62) Schnieder, L.; Meier, W.; Welge, K. H.; Ashfold, M. N. R.; Western, C. M. *J. Chem. Phys.* **1990**, *92*, 7027.
(63) Hwang, H. J.; El-Sayed, M. *Chem. Phys. Lett.* **1990**, *170*, 161.
(64) Wiley: W. C.; McLaren, I. H. *Rev. Sci. Instrum.* **1955**, *26*, 1150.
(65) Alexander, M. H.; Pouilly, B.; Duhoo, T. *J. Chem. Phys.* **1993**, *99*, 1752.
(66) Lambert, H. M.; Dagdigian, P. J.; Alexander, M. H. *J. Chem. Phys.* **1998**, *108*, 4460.
(67) Langford, S. R.; Regan, P. M.; Orr-Ewing, A. J.; Ashfold, M. N. R. *Chem. Phys.* **1998**, *231*, 245.
(68) Regan, P. M.; Ascenzi, D.; Clementi, C.; Ashfold, M. N. R.; Orr-Ewing, A. J. *Chem. Phys. Lett.* **1999**, *315*, 187.
(69) Alekseyev, A. B.; Liebermann, H. P.; Kokh, D. B.; Buenker, R. J. *J. Chem. Phys.* **2000**, *113*, 6174.
(70) Balakrishnan, N.; Alekseyev, A. B.; Buenker, R. J. *Chem. Phys. Lett.* **2001**, *341*, 594.
(71) Peoux, G.; Monnerville, M.; Duhoo, T.; Pouilly, B. *J. Chem. Phys.* **1997**, *107*, 70.
(72) Regan, P. M.; Langford, S. R.; Orr-Ewing, A. J.; Ashfold, M. N. R. *J. Chem. Phys.* **1999**, *110*, 281.
(73) Bickes, R. W.; Lantzsch, B.; Toennies, J. P.; Walaschewski, K. *Faraday Discuss. Chem. Soc.* **1973**, *55*, 167.
(74) Toennies, J. P.; Welz, W.; Wolf, G. *J. Chem. Phys.* **1979**, *71*, 614.
(75) Baumfalk, R.; Nahler, N. H.; Buck, U. *Faraday Disscus.* **2001**, *118*, 247.
(76) Baumfalk, R.; Nahler, N. H.; Buck, U. *J. Phys. Chem.* **2001**, *114*, 4755.
(77) Tarasova, E. I.; Ratner, A. M.; Stepanenko, V. N.; Fugol, I. Y.; Chergui, M.; Schwentner, N. *J. Chem. Phys.* **1993**, *98*, 7786.
(78) Slavíček, P.; Roeselová, M.; Jungwirth, P.; Schmidt, B. *J. Chem. Phys.* **2001**, *114*, 1539.
(79) Jaques, C.; L.Valachovic,; Ionov, S.; Bömer, E.; Wen, Y.; Segall, J.; Wittig, C. *J. Chem. Soc., Faraday Trans.* **1993**, *89*, 1419.
(80) Suzuki, T.; Katayanagi, H.; Heaven, M. C. *J. Phys. Chem.* **1997**, *101*, 6697.
(81) von Pietrowski, R.; Rutzen, M.; von Haeften, K.; Kakar, S.; Möller, T. *Z. Phys. D* **1997**, *40*, 22.
(82) Khriachtchev, L.; Pettersson, M.; Runeberg, N.; Lundell, J.; Räsänen, M. *Nature* **2000**, *406*, 874.
(83) Pettersson, M.; Nieminen, J.; Khriachtchev, L.; Räsänen, M. *J. Chem. Phys.* **1997**, *107*, 8423.
(84) Lundell, J.; Pettersson, M.; Khriachtchev, L.; Räsänen, M.; Chaban, G. M.; Gerber, R. B. *Chem. Phys. Lett.* **2000**, *322*, 389.
(85) Friedrich, B.; Herschbach, D. *J. Chem. Phys.* **1999**, *111*, 6157.
(86) Friedrich, B.; Herschbach, D. *J. Phys. Chem. A* **1999**, *103*, 10280.
(87) Loesch, H. J. *Annu. Rev. Phys. Chem.* **1995**, *46*, 555.
(88) Friedrich, B.; Herschbach, D. *J. Phys. Chem.* **1995**, *99*, 15686.
(89) Kim, W.; Felker, P. M. *J. Chem. Phys.* **1996**, *104*, 1147.
(90) Larsen, J. J.; Sakai, H.; Safvan, C. P.; Wendt-Larsen, I.; Stapelfeldt, H. *J. Chem. Phys.* **1999**, *111*, 7774.
(91) Friedrich, B. 2001. Unpublished results.
(92) Nahler, N. H.; Baumfalk, R.; Buck, U.; Friedrich, B.; Bihary, Z.; Gerber, R. B. *J. Chem. Phys.* **2002**. In press.
(93) Bihary, Z.; Gerber, R. B. 2002. Unpublished results.
(94) Oritigoso, J.; Rodriguez, M.; Gupta, M.; Friedrich, B. *J. Phys. Chem.* **1999**, *110*, 3870.
(95) Aker, P. M.; Germann, G. J.; Valentini, J. J. *J. Chem. Phys.* **1989**, *90*, 4795.
(96) Aker, P. M.; Germann, G. J.; Tabor, K. D.; Valentini, J. J. *J. Chem. Phys.* **1989**, *90*, 4809.
(97) Aker, P. M.; Valentini, J. J. *J. Phys. Chem.* **1993**, *97*, 2078.
(98) Briant, M.; Gaveau, M. A.; Fournier, P. R.; Mestdagh, J. M.; Visticot, J. P.; Soep, B. *Faraday Discuss.* **2001**, *118*, 209.